Rock and Soil Mechanics

Volume 43 | Issue 4 Article 8

6-9-2022

Parameter back-analysis of hardening soil model for granite residual soil and its engineering applications

Min ZHU
Key Laboratory of Coastal Urban Resilient Infrastructures of Ministry of Education, Shenzhen University, Shenzhen, Guangdong 518060, China

Xiang-sheng CHEN
Key Laboratory of Coastal Urban Resilient Infrastructures of Ministry of Education, Shenzhen University, Shenzhen, Guangdong 518060, China, xschen@szu.edu.cn

Guo-tao ZHANG
Key Laboratory of Coastal Urban Resilient Infrastructures of Ministry of Education, Shenzhen University, Shenzhen, Guangdong 518060, China

Xiao-chao PANG
China Academy of Railway Sciences (Shenzhen) Research and Design Institute Co., Ltd., Shenzhen, Guangdong 518060, China

See next page for additional authors

Custom Citation

ZHU Min, CHEN Xiang-sheng, ZHANG Guo-tao, PANG Xiao-chao, SU Dong, LIU Ji-qiang, . Parameter back-analysis of hardening soil model for granite residual soil and its engineering applications[J]. Rock and Soil Mechanics, 2022, 43(4): 1061-1072.

Parameter back-analysis of hardening soil model for granite residual soil and its engineering applications

Authors

Min ZHU, Xiang-sheng CHEN, Guo-tao ZHANG, Xiao-chao PANG, Dong SU, and Ji-qiang LIU

Rock and Soil Mechanics 2022 43(4): 1061−1072 ISSN 1000−7598
https: //doi.org/10.16285/j.rsm.2021.6062 rocksoilmech.researchcommons.org/journal

Parameter back-analysis of hardening soil model for granite residual soil and its engineering applications

ZHU Min[1, 2], CHEN Xiang-sheng[1, 2], ZHANG Guo-tao[1, 2], PANG Xiao-chao[3], SU Dong[1, 2], LIU Ji-qiang[4]

1. College of Civil and Transportation Engineering, Shenzhen University, Shenzhen, Guangdong 518060, China
2. Key Laboratory of Coastal Urban Resilient Infrastructures of Ministry of Education, Shenzhen University, Shenzhen, Guangdong 518060, China
3. China Academy of Railway Sciences (Shenzhen) Research and Design Institute Co., Ltd., Shenzhen, Guangdong 518060, China
4. China Railway Southern Investment Group Co., Ltd., Shenzhen, Guangdong 518060, China

Abstract: In recent years, construction works near the operating metro tunnel in granite residual soil have been gradually increasing, and the impact of these construction works on the safety of shield tunnel should not be ignored. Finite element method is an effective method to evaluate the influence of adjacent construction on shield tunnel, but its reliability highly depends on the reasonable selection of soil constitutive model and parameters. In this paper, the current situation of parameter selection of hardening soil model for granite residual soil is firstly reviewed. Then a back-analysis method for determining the parameters of granite residual soil based on the self-boring pressuremeter test (SBPMT) is proposed. Finally, the obtained back-analysis parameters are applied to the engineering case of foundation pit excavated overpass existing shield tunnel for method verification, and more reasonable values of parameters of hardening soil model for granite residual soil are determined. The results show that the strength parameters of hardening soil model for granite residual soil can be determined by laboratory tests, and the stiffness parameters of E_{50}^{ref}, $E_{\mathrm{oed}}^{\mathrm{ref}}$ and $E_{\mathrm{ur}}^{\mathrm{ref}}$ are the key parameters for the back-analysis. The ratio of E_{50}^{ref}: $E_{\mathrm{oed}}^{\mathrm{ref}}$: $E_{\mathrm{ur}}^{\mathrm{ref}}$ from 1:1:3 to 1:1:5 is suitable for engineering practice, and the value of E_{50}^{ref} ranges from 36 MPa to 43 MPa according to different ratios.

Keywords: granite residual soil; self-boring pressuremeter test; hardening soil model; parameter back-analysis; foundation excavation; shield tunnel

1 Introduction

The engineering projects near operating metro lines in prosperous urban area are growing annually in recent years, and their impacts on metro tunnel should not be ignored. The adjacent constructions alter the stress and displacement fields of the surrounding soil, resulting in structural deformation of the shield tunnel[1−2]. Excessive deformation may result in a variety of diseases, including segment cracking, joint opening, segment dislocation, water leakage, and track irregularity, which seriously threaten the operational security of the metro tunnel[3−4]. Many metro lines in Shenzhen pass through the granite residual soil layer, which is formed by weathered granite that has not been transported. Granite residual soil has the engineering properties of both cohesive and coarse-grained soils[5]. Due to its unique forming environment, complex material compositions, and structural properties[6], the shield tunnel in the residual soil layer is more susceptible to surrounding construction disturbances.

The finite element method is frequently used to evaluate the effect of adjacent construction on the shield tunnel[7−10]. The stress−strain relationship in granite residual soil is typically characterized by the hardening soil model (HS model, hereunder) and the hardening soil model with small strain stiffness (HSS model). The parameters of the constitutive models are mainly determined by laboratory tests of undisturbed samples[11−16]. However, engineering practice demonstrates that laboratory parameters may generate noticeable inaccuracies. To solve this problem, the self-boring pressuremeter test (SBPMT) has become an effective in-situ method for determining soil parameters because of its characteristics of small disturbance and large test depth[17−18]. In conjunction with cavity expansion theory and the finite element method, it is frequently used to back-analyze the parameters of different soil constitutive models, including Duncan-Chang model[19] and Cam-Clay model[20]. However, no investigation has been conducted into the back-analysis of HS model parameters for granite residual soil based on the SBPMT results.

A back-analysis method for determining parameters of HS model for residual soil is proposed in this paper based on well-documented SBPM test data, which is validated by the engineering case of foundation pit

Received: 13 July 2021 Revised: 05 October 2021
This work was supported by the Young Scholars of National Natural Science Foundation of China (52008263), the Foundation of China Railway Research Institute (2019YJ181) and the National Natural Science Foundation of China (51938008, 52090084).
First author: ZHU Min, male, born in 1990, PhD, Post doctor, research interests: foundation engineering, tunnel engineering, grouting. E-mail: zhuminfnf@163.com
Corresponding author: CHEN Xiang-sheng, male, born in 1956, PhD, Professor, PhD supervisor, Academician of Chinese Academy of Engineering, research interests: resilience of underground space, underground engineering, ground freezing method. E-mail: xschen@szu.edu.cn

construction overpass the existing metro tunnel in Shenzhen. Reasonable ranges of HS model parameters for residual soil are determined, which can provide reference for the safety impact assessment of subway security zone in granite residual soil layer.

2 Current situation of parameter selection of the HS model for granite residual soil

2.1 Applicability of the HS model for granite residual soil

Aiming at deformation control in the numerical analysis of urban subway security zone, the soil constitutive model needs to accurately reflect the mechanical behaviors that have direct effects on soil deformation. The basic mechanical parameters of granite residual soil are listed in Table 1, along with the application of several constitutive models. HS and HSS models incorporate the key aspects of M-C model, MCC model, and Duncan-Chang model, and enhance the capacity to explain nonlinear soil deformation, giving them broader engineering applicability.

Table 1 Mechanical properties of granite residual soil and applicability of constitutive models

Mechanical properties	M-C	MCC	Duncan-Chang	HS	HSS
Compressive hardening	√	√	√	√	√
Isobaric yield	×	√	×	√	√
Dilatancy	√	√	×	√	√
Stress path correlation	√	√	×	√	√
Loading and unloading stiffness difference	×	×	×	√	√
Small strain characteristics	×	×	×	×	√
Structural characteristics	×	×	×	×	×
Unsaturated characteristics	×	×	×	×	×

2.2 Parameter characteristics of the HS model obtained from laboratory tests

Table 2 summarizes HS model parameters for granite residual soil in the southeast coastal region of China as determined in laboratory tests[11−15], where ψ denotes the soil dilatancy angle; m denotes the power exponent reflecting the change of stiffness with stress; K_0^{nc} denotes the lateral pressure coefficient of soil mass; and R_f denotes the failure ratio. The main characteristics are as follows:

(1) The strength parameters vary greatly.

In the "*Design code for building foundation*" (DBJ15-31-2016)[21], the weathered granite with a standard penetration number N<40 is classified as the granite residual soil. According to Hong Kong design requirements and the study by Pun et al.[22], the cohesion c' of granite residual soil with N<40 ranges from 0 to 6 kPa, and the internal friction angle φ' ranges from 32° to 43°. The strength parameters show two different modes, including "small cohesion, large friction angle" mode and "large cohesion, small friction angle" mode.

Table 2 Parameters of HS model for granite residual soil in laboratory tests

Area	c' /kPa	φ' /(°)	ψ /(°)	E_{50}^{ref} /MPa	E_{oed}^{ref} /MPa	E_{ur}^{ref} /MPa	m	K_0^{nc}	R_f
Shenzhen	25.7	26.7	0.0	6.5	3.1	23.6	0.78	0.55	0.70
Shenzhen	8	32	0.0	7.5	7.5	25.5	0.72	0.47	0.89
Zhaoqing	22.0	28.0	7.5	11.2	4.1	33.6	0.41	0.53	0.91
Xiamen	25.1	15.1	0.0	9.3	5.7	32.9	0.80	0.70	0.97
Xiamen	30	23.4	0.0	12.0	12.0	30.0	0.80	0.60	0.95

(2) The stiffness parameters are relatively small.

The value of E_{50}^{ref} for granite residual soil measured by the laboratory test ranges from 6 to 12 MPa, E_{oed}^{ref} is about 0.5 to 1 time E_{50}^{ref}, and E_{ur}^{ref} is about 3 to 4 times E_{50}^{ref}. Due to the disturbance caused by the sampling, sample preparation, and saturation procedures, the stiffness parameters obtained by laboratory tests are relatively small, and soil deformation is substantially overestimated when employed in engineering calculations.

2.3 Parameters of the HS model used in engineering calculation

There are two ways used in engineering calculation to solve this problem. The first way is to obtain stiffness parameters for the HS model that are consistent with engineering experience through the back-analysis of a large number of engineering projects, and establish an empirical relationship with field test indicators (such as SPT blow count N). The second way is to directly calculate it using the HSS model[23], which takes small-strain stiffness characteristics into account. For the soft soil in Shanghai and Jinan, systematic research results have been obtained in term of HSS model[24−27]. With regard to granite residual soil, the same parameters as HS model are determined by laboratory test, and the small-strain stiffness parameters are obtained by field shear wave velocity test and indoor bending element test. Starting from the triaxial consolidation drainage curve and engineering examples, the characteristics of the above two parameter determination methods are discussed below:

2.3.1 Difference in CD triaxial test

Taking the parameters of reference [11] as an example (see group 2 of Table 2, the small strain parameters G_0^{ref} =60.3 MPa, $\gamma_{0.7}$ =3×10^{-4}), the CD triaxial test curve under the standard confining pressure of 100 kPa is calculated in the PLAXIS geotechnical test module. The calculated results are illustrated in Fig. 1. Curve (a) is the loading curve of HS model. Curves (b) and (c) correspond to the above two methods. The HSS model and HS model are adopted, respectively, and intersect at 50% failure load.

The HSS model takes the shear strain as the hardening parameter and modifies the hardening function by adding a correction coefficient h_i. Only in the small strain stage, h_i>1, the shear strain under the same eccentric stress is smaller than that of the HS model; when the tangent shear modulus G_t decays to G_{ur}, h_i=1, the HSS model is completely consistent with HS model. The critical shear strain γ_c at $G_t = G_{ur}$ is

$$\gamma_c = \frac{\gamma_{0.7}}{\alpha}\left(\sqrt{\frac{G_0}{G_{ur}}} - 1\right) \quad (1)$$

where G_0 is the initial shear modulus, α=0.385; $\gamma_{0.7}$ is the shear strain value when the secant shear modulus decays to 72.2% G_0; and $G_{ur} = E_{ur}/2(1+\nu_{ur})$ is the lower limit of shear stiffness attenuation.

According to Eq. (1), γ_c=0.11%. Compared with curve (a), the tangent stiffness of curve (b) under the same deviatoric stress increases significantly only within the influence range of small strain. The strain difference between curves (a) and (b) is mainly caused by the small strain section, which remains basically unchanged after γ_c>0.11%; the tangent stiffness of curve (c) increases as a whole, and the strain difference between curves (a) and (c) increases gradually with the increase of deviator stress.

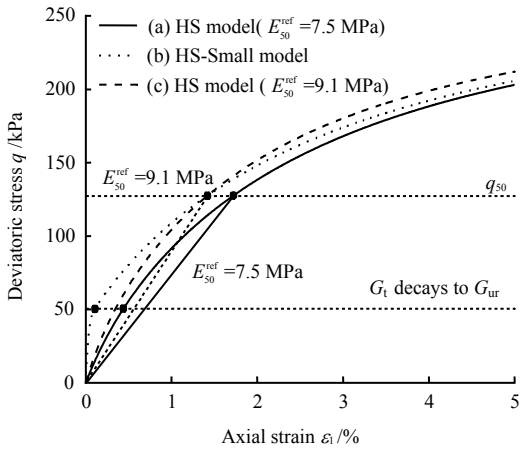

Fig. 1 Comparison of stress−strain relationship in drained triaxial test (Parameters from [11])

2.3.2 Engineering calculation

The details of engineering cases are listed in sections 3.1 and 3.2. Based on the parameters in section 2.3.1, E_{50}^{ref}, E_{oed}^{ref} and E_{ur}^{ref} increase to 45 MPa, 45 MPa and 135 MPa, respectively. The maximum heave amount of the tunnel is 31.5 mm and the maximum horizontal displacement of the retaining structure is 36.1 mm. For the HSS model, the parameters of the HS model are kept the same, and the small strain stiffness parameters are set as G_0=130 MPa, $\gamma_{0.7}$=3×10^{-4}. The maximum heave amount of the tunnel is 29.4 mm, and the maximum horizontal displacement of the retaining structure is 43.8 mm.

Figure 2 shows the nephogram of soil shear strain distribution under two parameter determination methods. The large value of shear strain calculated by the HS model is concentrated between 1% and 2%, only local strain near the retaining structure at the bottom of the foundation pit reaches 5%, and the overall distribution of soil shear strain is continuous. The distribution of shear strain calculated by the HSS model is more concentrated, and the larger value is concentrated between 3% and 5%. This is because the difference between the small strain stiffness G_0 and G_{ur} is too large when the laboratory E_{ur}^{ref} is used in the HSS model, resulting in the rapid attenuation of soil stiffness and local deformation.

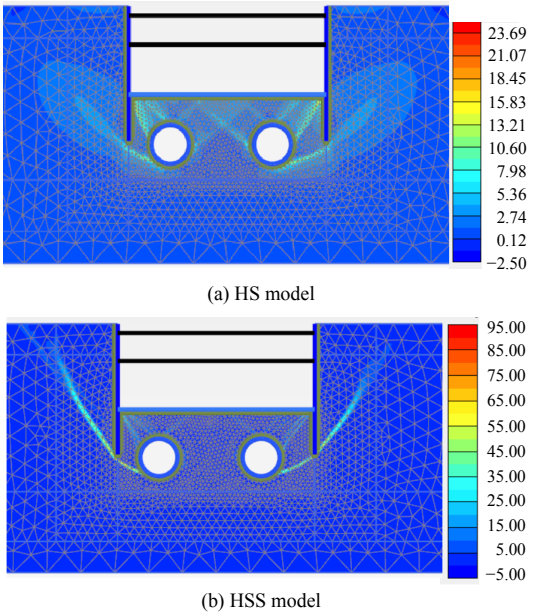

Fig. 2 Comparison of the shear strain nephogram between HS and HSS models (unit: 10^{-3})

2.4 Limitations of the current parameter determination methods

(1) Modifying the stiffness parameter E_{50}^{ref} of the HS model and establishing the empirical relationship with SPT blow count N requires a large number of engineering cases with detailed monitoring data, which is not applicable at the moment.

(2) When the HSS model is used for calculation, large errors appear in the obtained parameters, since the granite residual soil has strong structure, which greatly disturbs the undisturbed soil in the process of sampling, sample preparation and saturation in the laboratory test. Additionally, the parameters of small strain stiffness are also affected by a variety of factors, including the test method, stress path, saturation condition, and disturbance. The fluctuation range of G_0 and $\gamma_{0.7}$ is large[6, 26−34]. As shown in Fig. 3, the

parameter $\gamma_{0.7}$ varies greatly.

Therefore, certain limitation exists to directly determine the stiffness parameter such as E_{50}^{ref}, $E_{\mathrm{oed}}^{\mathrm{ref}}$, and $E_{\mathrm{ur}}^{\mathrm{ref}}$ by laboratory test, and there is no sufficient condition to establish the empirical relationship between E_{50}^{ref} and SPT blow count N. In order to solve the above problems, a back-analysis method of HS model parameters for granite residual soil based on SBPMTs is proposed.

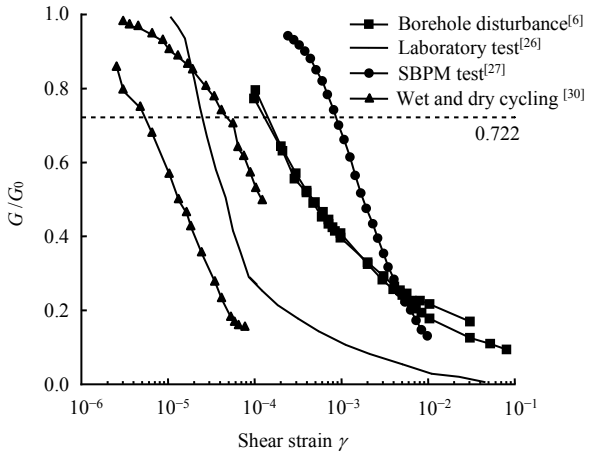

Fig. 3 Normalized curves of shear modulus for granite residual soil

3 Back-analysis of the parameters of the HS model for residual soil based on SBPMT

3.1 SBPMT

The data is from the SBPMT (hole 4) in Shenzhen Bay by institute of rock and soil mechanics, Chinese academy of sciences. Fig. 4 depicts *P-u* curves of granite residual soil at different depths of 17−20 m, which corresponds to the typical buried depth of metro tunnels. It can be seen that the shape of the *P-u* curve of residual soil at each depth is similar, and the overall stiffness of the curve is greater with the increase of depth. Figure 5 shows the incremental curve Δu-P of radial displacement under different depths and loads at all levels. When the load P<600 kPa, the displacement increment increases linearly with the increase of the load. When the load P>600 kPa, the displacement growth rate accelerates significantly, and the smaller the burial depth, the faster the displacement growth rate.

3.2 Back-analysis method

According to the SBPMT, an axisymmetric finite element model was established with PLAXIS 2D module, as shown in Fig. 6. The modeling range is 10 m× 30 m, the radius of the drilling hole a_0 is 41.5 mm, and the length of the loading device is 1.2 m. The minimum distance between the model boundary and the drilling position is 240 a_0. The central section is subjected to uniform expansion pressure. To minimize the influence of the boundary on the calculation results, static earth pressure is employed above and below the loading area instead of setting displacement limitations. The top boundary is free, the bottom boundary is completely fixed, and the left and right boundary are fixed in normal directions. The natural unit weight of granite residual soil γ_{unsat} =18 kN/m^3, the saturated unit weight γ_{sat} =19 kN/m^3, and the permeability coefficient k= 0.5 m/d.

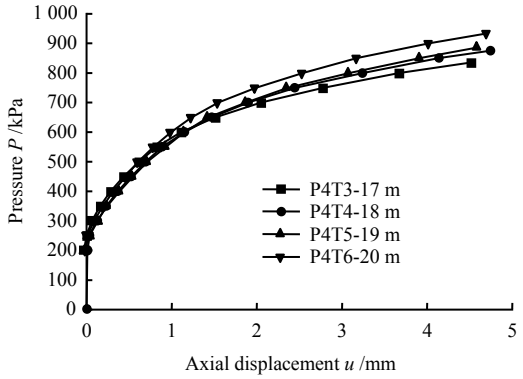

Fig. 4 *P-u* curves of SBPMTs (Borehole: P4)

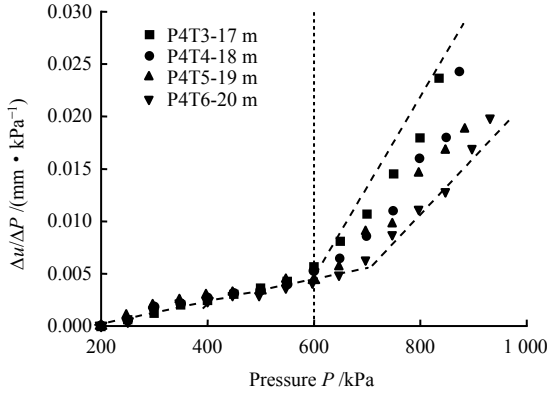

Fig. 5 Curves of incremental displacement under different loads (Borehole: P4)

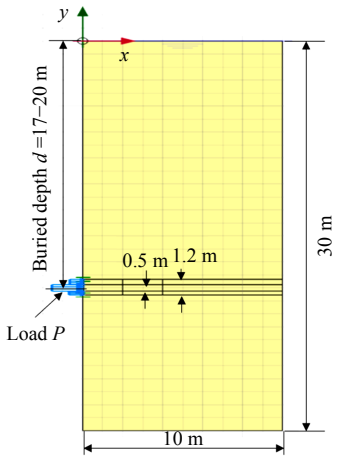

Fig. 6 Finite element model of the SBPMT

In order to verify the rationality of the finite element

model, the M-C model was used in the finite element analysis (parameters: cohersion c' =10.7 kPa, φ' =32°, dilatancy angle ψ =5°, effective elastic modulus E' = 50 MPa), and the simulated result was compared with the theoretical solution from Yu et al.[34], as shown in Fig. 7, the numerical solution (infinite length) is basically consistent with the theoretical solution. The numerical solution with a length of 0.5 m (about 6 times the diameter of the hole) shows a rigid loading effect, which is consistent with the conclusion drawn by Ajalloeian et al.[36].

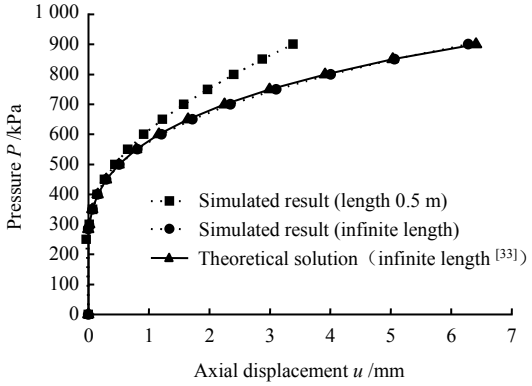

Fig. 7 Comparison of calculated *P-u* curves using M-C model and the theoretical solution

In order to obtain the actual HS model parameters of granite residual soil, the drainage conditions, parameter sensitivity, and evaluation indexes are discussed as follows:

3.2.1 Drained analysis is adopted and the calculated results are compared with the measured *P-u* curve at 250−600 kPa.

The loading rate of the SBPMT is fast, which is 4 kPa/s, while the permeability of granite residual soil is 0.5 m/d, which is between sand and clay, so the drainage condition was first determined. Analysis under complete drainage, solid-fluid coupling and undrained conditions were conducted with parameters c' =10.7 kPa, φ' =32°, ψ =5°, R_f =0.92, E_{50}^{ref} =45 MPa, E_{oed}^{ref} = 45 MPa, E_{ur}^{ref} =135 MPa, m=0.83, as shown in Fig. 8. Due to the strong permeability of residual soil, The results of solid-fluid coupling analysis is consistent with the drained analysis in spite of fast loading rate. The displacement development rate of undrained analysis is significantly faster than the measured curve. Therefore, drainage analysis can be used in the numerical simulation of SBPMT.

Figure 9 shows the comparison of the displacement increment curves obtained by the measured and numerical methods. When P<600 kPa, the results of the drained and fluid-solid coupling analysis are close to the measured curve. When P>600 kPa, the growth rate of the measured curve displacement is greatly accelerated. The shear strain at 600 kPa is between 3% and 4%, exceeding the influence range of small strain stiffness. The reasons for the change of displacement growth rate may be the structural failure of residual soil, the local permeability change caused by soil compression, and the boundary condition change caused by the failure of borehole structure. Considering the strict deformation control and small overall soil strain during the foundation pit construction in the subway security zone, it is appropriate to select the 250−600 kPa section of the measured *P-u* curve for the back-analysis.

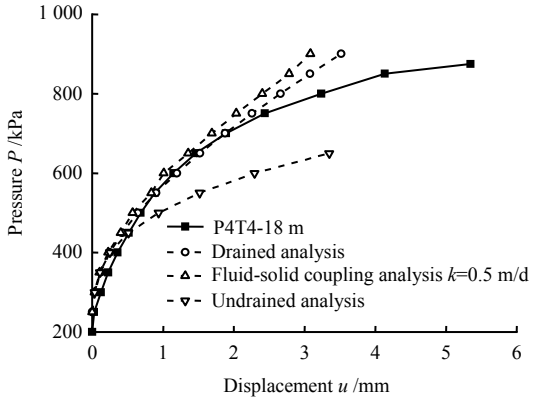

Fig. 8 *P-u* curves of the SBPMT under different drainage conditions

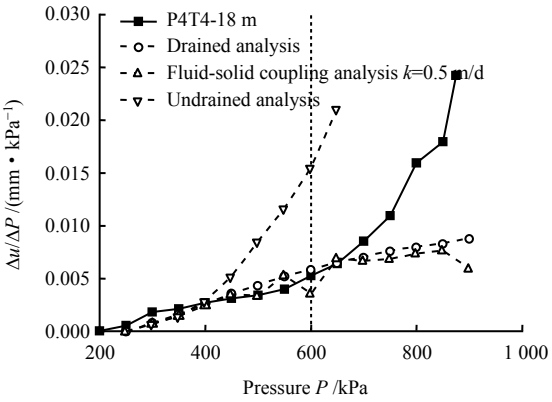

Fig. 9 Curves of incremental displacement of the SBPM test under different drainage conditions

3.2.2 The strength parameters are determined according to the laboratory test results, and the stiffness parameters are back-analyzed by the finite element model

It is impossible to back-analyze all the parameters because of too many parameters in HS model. Therefore, the sensitivity analysis is conducted firstly to determine the key parameters for the back-analysis. Taken the parameters in Section 3.2.1 as an example, the sensitivity of strength and stiffness parameters are analyzed. The given parameters are changed by −20%, −10%, −5%, 5%, 10%, and 20%, respectively, and the other parameters remain unchanged, the change rate of radial displacement u is calculated in the case that P=600 kPa. Figs. 10(a)

and 10(b) are the calculated sensitivity results of strength and stiffness parameters, respectively. On the whole, the stiffness parameters have a greater impact on the calculated results. Except for the effective internal friction angle φ', the other parameters are linearly related to the radial displacement u. Among the linear correlation parameters, only m is positively correlated with radial displacement, while the other parameters are negatively correlated with radial displacement. The stiffness parameters rank in an descending order of $E_{\text{oed}}^{\text{ref}}$, $E_{\text{ur}}^{\text{ref}}$, E_{50}^{ref}, m according to their influence on radial displacement.

According to the laboratory test results of undisturbed and remolded samples of granite residual soil carried out by Yu[13] and Pang[34], the strength parameters do not show much difference, indicating that the strength parameters of undisturbed and remolded samples are close and less affected by structural failure in the remolding process. Therefore, the strength parameters of in-situ undisturbed soil are determined by the laboratory triaxial test. Referring to the relevant literature, the experience in Hong Kong, and our triaxial undrained test result, the in-situ strength parameters in this paper are: c'=10.7 kPa, φ'=32°, ψ=5°. In addition, R_{f} is set at 0.92.

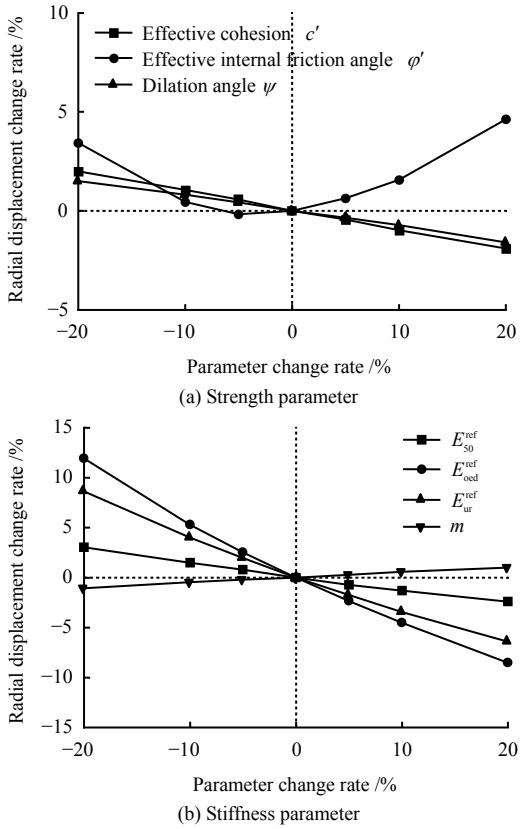

Fig. 10 The sensitivity of soil parameters to the displacement of SBPMT

For the stiffness parameters, they are arranged according to the parameter sensitivity. The back-analysis is mainly for the three parameters E_{50}^{ref}, $E_{\text{oed}}^{\text{ref}}$, and $E_{\text{ur}}^{\text{ref}}$, m=0.83. A total of 6 groups of commonly used ratios (E_{50}^{ref} : $E_{\text{oed}}^{\text{ref}}$: $E_{\text{ur}}^{\text{ref}}$), are set. The optimal values of E_{50}^{ref}, $E_{\text{oed}}^{\text{ref}}$, and $E_{\text{ur}}^{\text{ref}}$ for different ratios under the condition of m=0.83 were first determined, and then the m value was adjusted to verify its influence on the back-analysis results.

3.2.3 Euclidean distance is used as the evaluation index.

The sum of the Euclidean distance between the measured displacement and the simulated displacement at the 250−600 kPa is used as the evaluation index:

$$d = \sum_{P=250}^{600} \left| u_{P\text{m}} - u_{P\text{s}} \right| \tag{2}$$

where d is the evaluation index based on the cumulative Euclidean distance; $u_{P\text{m}}$ is the measured radial displacement at pressure P; $u_{P\text{s}}$ is the calculated radial displacement at pressure P. The smaller d value, the closer the calculated P-u curve to the measured one.

3.3 Results of the back-analysis

Firstly, the optimal values of E_{50}^{ref}, $E_{\text{oed}}^{\text{ref}}$, $E_{\text{ur}}^{\text{ref}}$ have been studied under the condition of m=0.83. Fig. 11 shows the results of E_{50}^{ref}, $E_{\text{oed}}^{\text{ref}}$, and $E_{\text{ur}}^{\text{ref}}$ parameters under different proportions of granite residual soil at a depth of 18 m (m=0.83). In the case that $E_{\text{oed}}^{\text{ref}}$ = $0.5\,E_{50}^{\text{ref}}$, the optimal E_{50}^{ref} value is generally greater. As $E_{50}^{\text{ref}}:E_{\text{ur}}^{\text{ref}}$ changes from 1:3 to 1:5, the optimal E_{50}^{ref} value gradually decreases.

Table 3 shows the optimal E_{50}^{ref} and corresponding cumulative Euclidean distance inversed from the measured curves of four groups of SBPMT at different depths from P4T3(17 m) to P4T6(20 m). As the test depth increases, the optimal stiffness parameters show a decreasing trend. Except for the discreteness of granite residual soil, the reason may be that the four tests were conducted in the same hole, from shallow to deep, and the previous tests caused a certain disturbance to the soil, which made the displacement growth rate of the later test curve change faster.

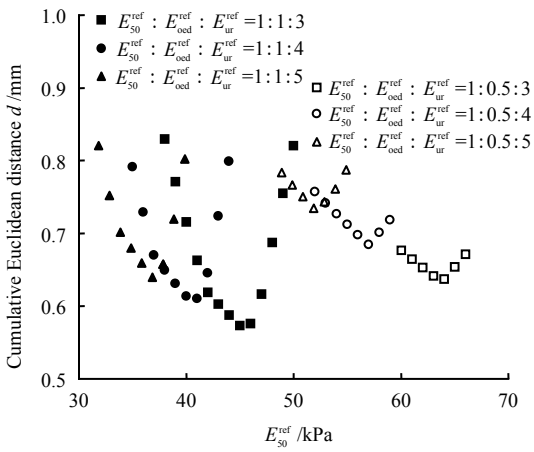

Fig. 11 Optimal E_{50}^{ref} under different proportions of the stiffness parameters (depth:18 m)

Table 3 Summary of optimal E_{50}^{ref} under different proportions of the stiffness parameters

E_{50}^{ref} : E_{oed}^{ref} : E_{ur}^{ref}	Parameter values for different depths (m)									
	17		18		19		20		average	
	E_{50}^{ref} /MPa	d /mm	E_{50}^{ref} /MPa	d /mm	E_{50}^{ref} /MPa	d /mm	E_{50}^{ref} /MPa	d /mm	E_{50}^{ref} /MPa	d /mm
1:1:3	56	0.13	45	0.57	37	0.74	31	0.96	42.3	0.60
1:1:4	51	0.15	41	0.61	32	0.82	27	0.98	37.8	0.64
1:1:5	46	0.18	37	0.64	34	0.41	28	0.56	36.3	0.45
1:0.5:3	80	0.17	64	0.64	57	0.41	48	0.56	62.3	0.45
1:0.5:4	72	0.22	57	0.68	51	0.45	42	0.59	55.5	0.49
1:0.5:5	67	0.25	52	0.73	47	0.50	38	0.64	51.0	0.53

Taking the optimal parameter E_{50}^{ref}=42.3 MPa under the condition of E_{50}^{ref} : E_{oed}^{ref} : E_{ur}^{ref} =1:1:3 as an example, the influence of m are investigated. The cumulative Euclidean distance of 17−20 m when m is 0.4, 0.6, 0.8 and 1.0 is 0.92 mm, 0.92 mm, 0.92 mm and 0.93 mm, respectively, indicating that m has a relatively small effect.

4 Engineering verification

To validate the engineering applicability of the HS model parameters in the granite residual soil based on back-analysis of SBPMT, an engineering case of foundation pit excavation overpass the metro tunnel in Shenzhen was selected for verification.

4.1 Project overview

The total length of the foundation pit in Shenzhen is 369.3 m. As shown in Fig. 12, the width of the standard section is 32.0 m, and the depth of the foundation pit is about 13.77 m. The main retaining structure consists of the 800 mm thick underground diaphragm wall (depth of 21 m), one concrete support (6 m interval), and one steel support (3 m interval). The longitudinal slope rate of the underlying shield tunnel is 1%, and it passes through the structural floor in a parallel way.

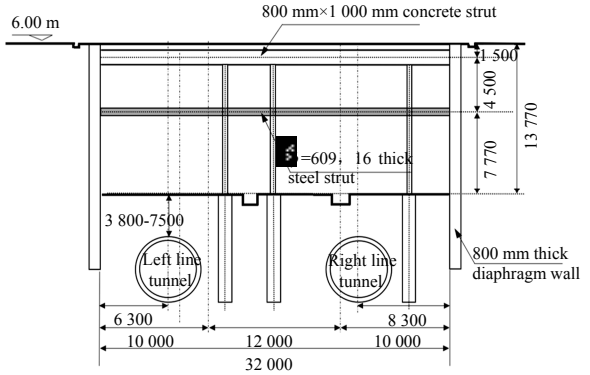

Fig. 12 Typical profile of the foundation pit (unit: mm)

The geological profile of the foundation hole is shown in Fig. 13. From top to bottom, the soil strata consist primarily of fill, gravelly clay, and weathered granite with varying weathering degrees. Groundwater is made up of pore water and fissure water. The covering depth of the shield tunnel is 17.2−21.7 m and 3.8−7.5 m after excavation. The physical and mechanical indexes of each soil layer are shown in Table 4.

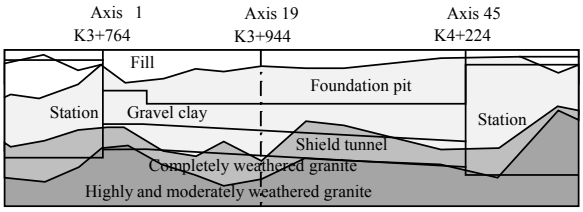

Fig. 13 Longitudinal geological profile

Table 4 Physical and mechanical indexes of the soil layers

Soil layer	Water content w /%	Natural unit weight γ/(kN • m^{-3})	Permeability coefficient k /(m • d^{-1})	SPT N
Fill	24.2	19.1	0.3	14.0
Gravel clay	27.8	18.0	0.5	25.3
Completely weathered granite	25.3	18.3	0.8	53.8
Highly weathered granite	22.8	18.7	2.0	–

4.2 Finite element model

Since the foundation pit and the tunnel are collinear for a long distance, and the conventional section excavation method is adopted, combined with the field operations, axis 19 in Fig. 13 is selected to establish the 2D finite element model, as shown in Fig. 14. The left and right boundaries are 50 m away from the diaphragm walls of the foundation pit to reduce the boundary effect, which is over three times the excavation depth. Considering that the strata below the highly weathered granite retain the original rock characteristics, which has good physical and mechanical properties and has little impact on the deformation of foundation pit and tunnel, the highly weathered granite is set at the bottom of the model. The geometric size is 132 m×40 m, which is divided into 6 769 elements and 55 354 nodes. The horizontal displacement is constrained at the left and right boundaries, and the bottom boundary is fixed. The top and side boundaries allow free drainage, and the bottom is impervious. The water level line is 3 m below the surface. The depth of the diaphragm wall is 21 m, the excavation depth is 13.77 m, the tunnel burial depth is 19 m, and the top surface of the tunnel

is 5.23 m away from the base slab.

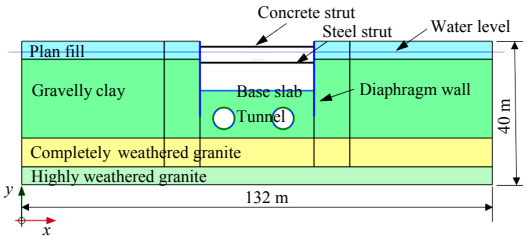

Fig. 14 Finite element model

The soil layers from top to bottom are the plain fill, gravelly clay, completely weathered granite, and highly weathered granite, with thicknesses of 5, 22, 8, and 5 m, respectively. The gravelly clay and completely weathered granite are unified as granite residual soil. The constitutive model adopts HS model, whose parameters are determined according to the back-analysis results in Section 2, where c' =10.7 kPa, φ' =32°, ψ =5°, R_f =0.92, K_0^{nc} =0.47, v_{ur} =0.2, p^{ref} =100 kPa, and m= 0.83. The other stiffness parameters, 6 groups in total, are summarized in Table 5.

The M-C model is used for plain fill and highly weathered granite, with the parameters for plain fill E' =28 MPa, v =0.3, c' =0 kPa, φ' =30° and highly weathered granite E' =250 MPa, v =0.2, c' =35 kPa, φ' =39°.

The structural parameters are shown in Table 6. The tunnel has an effective stiffness ratio of 0.7 and an interface coefficient of R_{inter} =0.65. The conditions corresponding to each analysis step of the numerical model are shown in Table 7. The water level in the pit is reduced to the excavation depth, and drainage analysis using steady-state seepage is adopted.

Table 5 Stiffness parameters of granite residual soil

Serial number	E_{50}^{ref} /MPa	E_{oed}^{ref} /MPa	E_{ur}^{ref} /MPa
1	42.3	42.3	126.9
2	37.8	37.8	151.2
3	36.3	36.3	181.5
4	62.3	31.2	186.9
5	55.5	27.8	222.0
6	51.0	25.5	255.0

Note: The parameters of gravelly clay and fully weathered rock are not distinguished in this paper.

Table 6 Structural parameters

Structure type	Size	Element type	E /GPa	v	R_{inter}
Diaphragm Wall	Thickness 800 mm	Plate	30	0.2	1
Base slab	Thickness 1 000 mm	Plate	30	0.2	1
Concrete strut	800 mm×1 000 mm	Anchor	30	0.2	-
Steel strut	Diameter 609 mm, thickness 16 mm	Anchor	210	0.3	-
Tunnel lining	Diameter 6 m, thickness 0.35 m	Plate	24.2	0.2	0.65

Table 7 Construction procedures

Analysis step	Construction work
1	Balance earth pressure
2	Excavate Tunnel
3	Excavate the first layer 1.8m
4	Cast concrete strut
5	Excavate the second layer 4.2 m
6	Install steel strut
7	Excavate the third layer 7.7 m
8	Construct base slab

4.3 Analysis of the calculation results

Figure 15 shows the comparison between the measured and calculated values of left and right tunnels during the whole construction process with $E_{50}^{ref} : E_{oed}^{ref} : E_{ur}^{ref} = 1:1:3$. Taking the left tunnel as an example, after the excavation of the first and second layers (total depth of 6 m), the heave of the tunnel crown is 8.5 mm. After the excavation of the third layer (total depth of 13.7 m), the crown heave reaches 28.6 mm. The excavation of the third layer has a significant effect on the tunnel heave. When the third layer of the axis 16−22 was completely excavated, the calculated value approached the measured value, indicating that the plain strain assumption is suitable, and the 2D model can simplify the calculation without significant error.

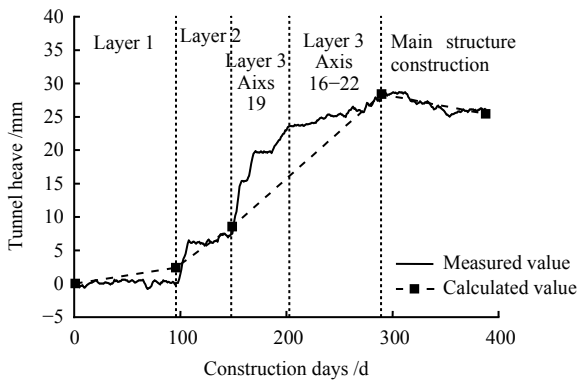

(a) Left tunnel

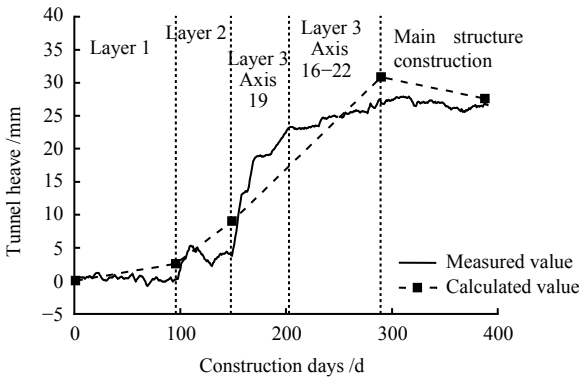

(b) Right tunnel

Fig. 15 The heave of shield tunnel crown during the whole construction process

The time point was selected when the soil excavation of the third layer of axis 16−22 was completed in the actual working condition (at this time, the measured tunnel heave reached the maximum). A comparative analysis was carried out under different stiffness parameter ratios. The lateral displacement of the right diaphragm wall is shown in Fig. 16. The shapes of the measured curve and the simulated curve are similar. When $E_{50}^{\mathrm{ref}}:E_{\mathrm{oed}}^{\mathrm{ref}}$=1:1, the maximum lateral displacement of the diaphragm wall is 34 mm. When $E_{50}^{\mathrm{ref}}:E_{\mathrm{oed}}^{\mathrm{ref}}$ = 1:0.5, the maximum lateral displacement is 25 mm, and the measured value is 23.8 mm. When $E_{50}^{\mathrm{ref}}:E_{\mathrm{oed}}^{\mathrm{ref}}$ is fixed, the maximum lateral displacement has no obvious change. Since the 2D model does not consider the influence of soil excavation and structure construction sequence, the calculated deformation of the diaphragm wall is larger and the position of the maximum value is lower.

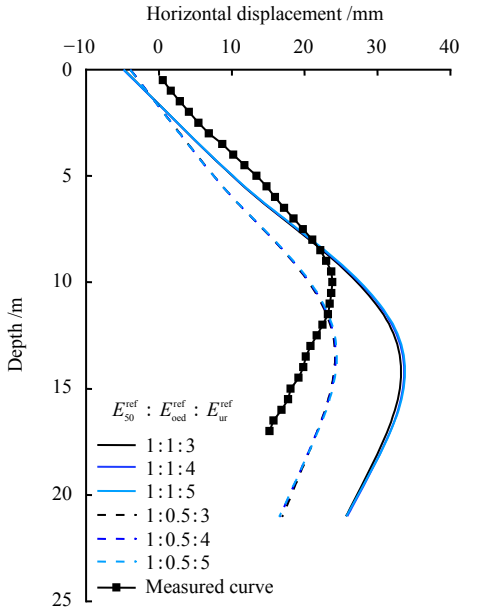

Fig. 16 Horizontal displacement of the diaphragm wall

The comparison between the calculated and measured values of the shield tunnel heave in polar coordinates is shown in Fig.17, where the circumferential coordinate represents the angle, and the radial coordinate represents the tunnel heave amount. Similar to the lateral displacement of the diaphragm wall, the heave amount of the tunnel at $E_{50}^{\mathrm{ref}}:E_{\mathrm{oed}}^{\mathrm{ref}}$=1:1 is larger than that at $E_{50}^{\mathrm{ref}}:E_{\mathrm{oed}}^{\mathrm{ref}}$=1:0.5, and it is in good agreement with the measured value. When $E_{50}^{\mathrm{ref}}:E_{\mathrm{oed}}^{\mathrm{ref}}$ is fixed, with the increase of $E_{50}^{\mathrm{ref}}:E_{\mathrm{ur}}^{\mathrm{ref}}$, the overall change of the tunnel heave is small. But the difference of the heave at the symmetrical position along the vertical axis (90°−270° axis) decreases, indicating that the inclination of the tunnel decreases slightly in the heave process. The right tunnel heave is slightly larger than that of the left tunnel, because it is closer to the center of the foundation pit, and is affected by the unloading effect more obviously.

Except for the location of the bottom of foundation pit near the diaphragm wall, the larger values of the soil shear strain near the foundation pit and tunnel under each group of parameters are between 0.3% and 1.5%, which is in line with the shear strain range back analyzed by SBPMT. In summary, the ratio of the HS stiffness parameters for granite residual soil can be set as $E_{50}^{\mathrm{ref}}:E_{\mathrm{oed}}^{\mathrm{ref}}:E_{\mathrm{ur}}^{\mathrm{ref}}$=1:1:3−1:1:5, which is more suitable for engineering practice. The E_{50}^{ref} value ranges from 36 to 43 MPa according to different ratios.

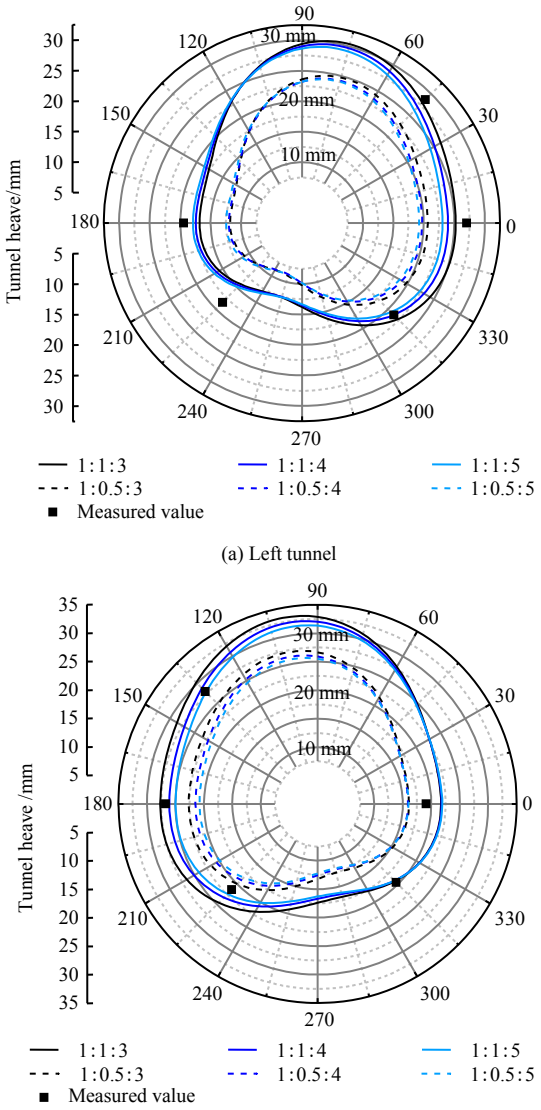

Fig. 17 Maximum heave of the shield tunnel section

4.4 Comparison of different constitutive models

In order to study the influence of different constitutive

models, the hardened soil (HS) model, the modified Cam-Clay (MCC) model, and the Mohr-Coulomb (M-C) model were selected for finite element calculation. The parameters of each model are as follows:

(1) HS model: c' =10.7 kPa, φ' =32°, ψ =5°, R_f = 0.92, K_0^{nc} =0.47, ν_{ur} =0.2, p^{ref} =100 kPa, m=0.83, E_{50}^{ref} : E_{oed}^{ref} : E_{ur}^{ref} =1 : 1 : 3, E_{50}^{ref} =42.3 MPa;

(2) MCC model: M=1.279, e_0 =1.02, λ =0.025, κ =0.005, ν =0.2;

(3) M-C model: c' =10.7kPa, φ' =32°, ψ =5°, E' =48 MPa, ν =0.2.

Figure 18 indicates the *P-u* curves calculated by using the three constitutive models in the finite element model of the SBPMT (depth of 20 m). The three curves are relatively close.

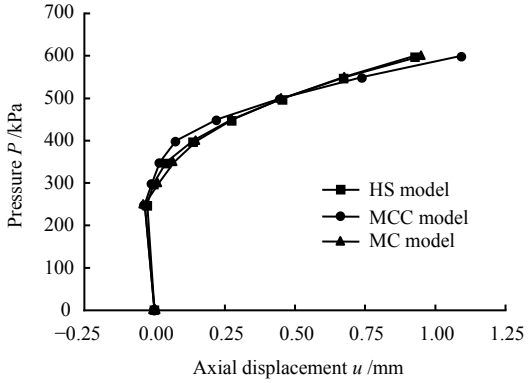

Fig. 18 *P-u* curves of SPBM tests under different constitutive models and parameters

Table 8 lists the calculated results obtained by using the three constitutive models in the engineering example. For tunnel heave, the predicted values of HS model and MCC model are close to the measured values, while the predicted values of the M-C model are too large, mainly because the M-C model cannot consider the difference between soil loading and unloading stiffness. For the maximum lateral displacement of the retaining structure, the predicted values of the three models are almost the same. For the maximum ground settlement, the overall prediction effect of HS model is good, and the prediction value of MCC model is too large. This is because the shear dilatancy of soil cannot be considered under the normal consolidation state of MCC model, while the contents of coarse and fine particles of granite residual soil are large, showing the properties of some sandy soil and strong shear dilatancy. Generally, the calculation results of the HS model are in good agreement with the measured data.

Table 8 Calculated results of engineering case using different constitutive models

Constitutive model	Maximum heave (left tunnel) /mm	Maximum lateral displacement of retaining structure /mm	Maximum ground settlement /mm
HS model	28.4	34.0	26.4
MCC model	28.2	30.0	52.9
MC model	53.5	29.7	14.4
Measured	28.6	23.8	21.6

4.5 Limitations of the back-analysis method

The stiffness parameters of HS model are back-analyzed by SBPMT, and are used for the safety impact assessment of subway security zone. Its limitations are as follows:

(1) The influence of strength parameters is not considered.

(2) The stress path of the SBPMT is lateral loading, while the stress path of foundation excavation is mainly unloading. The influence of the different stress paths on the soil mechanical properties is not fully considered.

(3) The influence of structure property, small strain characteristics, and unsaturated characteristics of granite residual soil are not taken into account.

5 Conclusions

A back-analysis method for determining the parameters of the hardening soil model for granite residual soil is developed based on the SBPMT, which is validated according to the engineering case of foundation pit overpass the existing metro tunnel in Shenzhen. The main conclusions are as follows:

(1) The stiffness parameters of the hardening soil model for granite residual soil obtained by the laboratory triaxial test are small, which means they cannot be directly used in engineering calculations. When using the hardening soil model with small strain stiffness, the small strain stiffness parameters are difficult to obtain accurately and have large impacts on the calculation results.

(2) According to the measured curve of SBPMT, when the finite element method is used to back analyze the parameters of HS model of residual soil, the influence of the stiffness parameter on the back-analysis results is generally greater than that of the strength parameters. The strength parameters can be determined by triaxial test. The stiffness parameters are E_{oed}^{ref}, E_{ur}^{ref}, E_{50}^{ref} and m in descending order of their influence on the *P-u* curve of the SBPMT. The optimal E_{50}^{ref} at E_{50}^{ref} : E_{oed}^{ref} =1 : 1 is generally less than that at E_{50}^{ref} : E_{oed}^{ref} =1 : 0.5. When E_{50}^{ref} : E_{ur}^{ref} varies from 1 : 3 to 1 : 5, the optimal E_{50}^{ref} decreases gradually.

(3) According to the SBPMT and the back-analysis results of engineering case, the HS model of granite residual soil in Shenzhen can be taken as c'=10.7 kPa, φ'=32°, ψ=5°, R_f=0.92, m=0.83, E_{50}^{ref} : E_{oed}^{ref} : E_{ur}^{ref} is 1:1:3−1:1:5, and the value of E_{50}^{ref} ranges from 36 to 43 MPa.

(4) In the future, the strength parameters, small strain characteristics, and the structure characteristics of granite residual soil, as well as the effect of the in-situ test stress path on the back-analysis results should be further investigated, and an empirical relationship between the constitutive model parameters of granite residual soil and the commonly used in-situ test indexes (SPT blow count N, etc.) should be established to facilitate the popularization and application of engineering projects.

References

[1] XU Si-fa, ZHOU Qi-hui, ZHENG Wen-hao, et al. Influences of construction of foundation pits on deformation of adjacent operating tunnels in whole process based on monitoring data[J]. Chinese Journal of Geotechnical Engineering, 2021, 43(5): 804−812.

[2] DING Zhi, ZHANG Xiao, LIANG Fa-yun, et al. Research and prospects regarding the effect of foundation pit excavation on an adjacent existing tunnel in soft soil[J]. China Journal of Highway and Transport, 2021, 34(3): 50−70.

[3] DONG Fei, FANG Qian, ZHANG Ding-li, et al. Analysis on defects of operational metro tunnels in Beijing[J]. China Civil Engineering Journal, 2017, 50(6): 104−113.

[4] ZHU M, GONG X N, GAO X, et al. Remediation of damaged shield tunnel using grouting technique: Serviceability improvements and prevention of potential risks[J]. Journal of Performance of Constructed Facilities, 2019, 33(6): 04019062.

[5] QIAN Z, RAHARDJO H, SATYANAGA A. Variability in unsaturated hydraulic properties of residual soil in Singapore[J]. Engineering Geology, 2016, 209: 21−29.

[6] AN Ran, LI Cheng-sheng, KONG Ling-wei, et al. Effects of drilling disturbance and unloading lag on in-situ mechanical characteristics of granite residual soil[J]. Chinese Journal of Geotechnical Engineering, 2020, 42(1): 109−116.

[7] HUANG Hong-wei, HUANG Xu, SCHWEIGER F H. Numerical analysis of the influence of deep excavation on underneath existing road tunnel[J]. China Civil Engineering Journal, 2012, 45(3): 182−189.

[8] ZHENG Gang, LIU Qing-chen, DENG Xu. Numerical analysis of effect of excavation on underlying existing metro tunnel and deformation control[J]. Rock and Soil Mechanics, 2013, 34(5): 1459−1468.

[9] CHEN R P, MENG F Y, LI Z, et al. Investigation of response of metro tunnels due to adjacent large excavation and protective measures in soft soils[J]. Tunnelling and Underground Space Technology, 2016, 58: 224−235.

[10] CHEN Shuan, WU Huai-na, CHEN Ren-peng, et al. Research on deformation of collinear tunnel induced by overlying long-distance excavation[J]. Journal of Shanghai Jiao Tong University, 2021, 55(6): 698−706.

[11] YE Yue-hong. Influence of construction of open-cut tunnelling on uplift displacement of the underneath metro tunnel and its control measures[D]. Hangzhou: Zhejiang University, 2017.

[12] PANG Xiao-chao, HUANG Jun-jie, SU Dong, et al. Experimental study on parameters of the hardening soil model for undisturbed granite residual soil in Shenzhen[J]. Rock and Soil Mechanics, 2018, 39(11): 4079−4085.

[13] YU Gang. Structural characterization and hardening soil model parameters analysis of granite residual soil[D]. Wuhan: Huazhong University of Science and Technology, 2019.

[14] NIU Hao. Mechanical test research of the granite residual soil considering small strain stiffness and its engineering application[D]. Quanzhou: Huaqiao University, 2017.

[15] LIN Qiao-yu. Study and engineering application of HSS model parameters of Xiamen granite residual soil[D]. Quanzhou: Huaqiao University, 2019.

[16] XIE Sheng-wei. Study on deformation mechanism of underlying tunnel caused by excavation and unloading of long distance foundation pit in residual soil layer[D]. Changsha: Hunan University, 2020.

[17] HAO Dong-xue. Study on cavity expansion theory and numerical analysis of self-boring pressuremeter test[D]. Dalian: Dalian University of Technology, 2008.

[18] HAO Dong-xue, CHEN Rong, LUAN Mao-tian, et al. Research development of estimation for soil properties from SBPM[J]. Chinese Journal of Computational Mechanics, 2011, 28(3): 452−460.

[19] LIU Xiao-sheng, WANG Xiao-gang, MA Huai-fa, et al. Study on back-analysis method of constitutive parameters for Duncan-Chang model based on in -situ pressuremeter tests[J]. Chinese Journal of Geotechnical Engineering, 2004, 26(5): 601−606.

[20] RANGEARD D, HICHER P Y, ZENTAR R. Determining soil permeability from pressuremeter tests[J]. International

Journal for Numerical Analytical Methods in Geomechanics, 2003, 27(1): 1−24.

[21] Department of housing and urban rural development of Guangdong Province. DBJ15-31−2016 Design code for building foundation[S]. Beijing: China Architecture & Building Press, 2017.

[22] PUN W K, HO K K S. Analysis of triaxial tests on granite saprolite performed at public works central laboratory (discussion note DN 4/96)[R]. Hong Kong: Geotechnical Engineering Office, Hong Kong Government of the Special Administrative Region, 1996.

[23] BENZ T. Small-strain stiffness of soils and its numerical consequences[M]. Stuttgart: University of Stuttgart, 2006.

[24] WANG Wei-dong, WANG Hao-ran, XU Zhong-hua. Study of parameters of HSS model used in numerical analysis of excavations in Shanghai area[J]. Rock and Soil Mechanics, 2013, 34(6): 1766−1774.

[25] LIANG Fa-yun, JIA Ya-jie, DING Yu-jin, et al. Experimental study on parameters of HSS model for soft soils in Shanghai[J]. Chinese Journal of Geotechnical Engineering, 2017, 39(2): 269−278.

[26] LI Lian-xiang, LIU Jia-dian, LI Ke-jin, et al. Study of parameters selection and applicability of HSS model in typical stratum of Jinan[J]. Rock and Soil Mechanics, 2019, 40(10): 4021−4029.

[27] GU Xiao-qiang, WU Rui-tuo, LIANG Fa-yun, et al. On HSS model parameters for Shanghai soils with engineering verification[J]. Rock and Soil Mechanics, 2021, 42(3): 833−845.

[28] SANTOS J A, CORREIA A G. Reference threshold shear strain of soil. Its application to obtain a unique strain-dependent shear modulus curve for soil[C]//15th International Conference SMGE. Istanbul: A.A. Balkema, 2001.

[29] NG C W W, PUN W K, PANG R P L. Small strain stiffness of natural granitic saprolite in Hong Kong[J]. Journal of Geotechnical and Geoenvironmental Engineering, 2000, 126(9): 819−833.

[30] NG C W W, WANG Y. Field and laboratory measurements of small strain stiffness of decomposed granites[J]. Soils and Foundations, 2001, 41(3): 57−71.

[31] WANG Y, NG C W W. Effects of stress paths on the small-strain stiffness of completely decomposed granite[J]. Canadian Geotechnical Journal, 2005, 42(4): 1200−1211.

[32] NG C W W, LEUNG E H Y. Determination of shear-wave velocities and shear moduli of completely decomposed tuff[J]. Journal of Geotechnical and Geoenvironmental Engineering, 2007, 133(6): 630−640.

[33] YIN Song, KONG Ling-wei, ZHANG Xian-wei. Experimental study on stiffness characteristics of residual soil at small strain under hot and rainy climate[J]. Chinese Journal of Geotechnical Engineering, 2017, 39(4): 743−751.

[34] PANG Xiao-chao. Experimental study and constitutive modelling of Shenzhen natural completed decomposed granite[D]. Beijing: China Academy of Railway Sciences, 2011.

[35] YU H S, HOULSBY G T. Finite cavity expansion in dilatant soils: loading analysis[J]. Geotechnique, 1991, 41(2): 173−183.

[36] AJALLOEIAN R, YU H S. Chamber studies of the effects of pressuremeter geometry on test results in sand[J]. Geotechnique, 1998, 48(5): 621−636.